INTERNATIONAL JOURNAL OF PRECISION ENGINEERING AND MANUFACTURING-GREEN TECHNOLOGY Vol. 3, No. 1, pp. 67-74 JANUARY 2016 / 67
DOI: 10.1007/s40684-016-0009-3 ISSN 2288-6206 (Print) / ISSN 2198-0810 (Online)

Eddy Current Damper Type Reaction Force Compensation Mechanism for Linear Motor Motion Stage

Hyeong-Joon Ahn[1,#]

1 Department of Mechanical Engineering, Soongsil University, 369, Sangdo-ro, Dongjak-gu, Seoul, 06978, South Korea
Corresponding Author / Email: ahj123@ssu.ac.kr, TEL: +82-2-820-0654, FAX: +82-2-820-0668

KEYWORDS: Linear motor motion stage, Reaction force compensation, Eddy current damper

The base vibration of a linear motor motion stage has been reduced with a passive reaction force compensation (RFC) mechanism based on a movable magnet track and springs. This paper presents the design procedure of an eddy-current damper (ECD) type RFC mechanism for a linear motor motion stage. The RFC mechanism with a movable magnet track and an ECD can overcome the disadvantages of the spring based RFC mechanism such as resonance and difficulty of assembly due to springs. A lumped parameter model for the ECD type RFC mechanism is derived considering sinusoidal magnetic flux density and the effective width of the ECD according to magnet track motion. Then, an iterative design procedure for ECD type RFC mechanisms is proposed to meet system requirements such as the transmission ratio of the reaction force and the maximum magnet track motion. Finally, a design example illustrates the effectiveness of the proposed design procedure for an ECD type RFC mechanism.

Manuscript received: June 24, 2015 / Revised: December 6, 2015 / Accepted: December 7, 2015

NOMENCLATURE

B : Flux density in the magnet track
c_{MT} : Damping of the RFC mechanism
d : Location of ECD
f_{ECD} : Force of ECD
f_f : Thrust force for mover friction
f_{fc} : Coulomb friction force
f_{fs} : Difference between max static and Coulomb friction forces
f_m : Thrust force for mover motion profile
f_T : Thrust force
f_{TR} : Transmitted force
k_{MT} : Stiffness of the RFC mechanism
k_v : Viscous friction coefficient of mover
l : Height of ECD
m_{Base} : Mass of system base
m_D : Dummy mass for magnet track
m_M : Mass of mover
m_{MT} : Mass of magnet track
n_s : Exponent coefficient for stribeck effect
sgn : Sign function
t : Thickness of ECD
T_a : Acceleration time (constant acceleration)
T_{dw} : Dwell time (zero velocity)
T_r : Run time (zero acceleration or constant velocity)
v_s : Stribeck velocity
w : Width of ECD
w_e : Effective width of ECD
x_M : Position of mover
x_{MT} : Position of magnet track
α : Geometric coefficient
σ : Conductivity of the conductor

1. Introduction

Moving mass and working area increases associated with the enlarged size of display panels and the improved productivity of the semiconductor industry need rapid and high precision motion stages. For example, semi-conductor lithography systems are specified s to be both ultra-precise and fast moving in very long strokes such as 1 nm accuracy and 230 wafers/hour over a 2 m stroke.[1]

Residual vibration due to rapid motion has a bad influence on both

quality and process time, as well as the life of manufacturing equipment. Rapid motion induces large reaction force and the system base oscillates either with substantial amplitude or for a long time. Therefore, many resources such as time, materials and CO^2 can be saved by reducing these residual vibrations.

Two main approaches are currently being used to reduce the residual vibration of the motion control system: software and hardware approaches. Software approaches can be divided into input shaping[2] and advanced control.[3] Alternatively, the hardware approach can intrinsically separate the excitation source of the vibration by force balancing or reaction force compensation.[4]

There are two main RFC methodologies to lower the vibration of the motion system.[5-7] One is to build a separate mechanical structure for an independent path of the reaction force.[5] The other is to install another motion stage to generate a counter force against the reaction force.[6,7]

A passive RFC mechanism with a movable magnet track and springs can reduce the base vibration of a linear motor motion stage considerably.[8] Since the magnet track oscillates according to the reaction force, only the spring force is transferred to the system base.[9] In addition, a passive RFC mechanism can be designed to consider the dynamic characteristics of the system base.[10] Furthermore, an active RFC mechanism can meet design requirements against motion profile variations.[11]

A RFC mechanism with a movable magnet track and an ECD (or conductor plate) can reduce the disadvantages of the spring based RFC mechanism such as resonance and difficulties of both assembly and design due to the springs.[12] In addition, the force transmission ratio and magnet track displacement can be adjusted by changing the shape and location of the conductor plate.

Eddy current dampers (ECD) are used to reduce the vibration of mechanical structures.[13-16] ECDs consist of magnets and a conductive metal plate. A permanent or electro-magnet with or without back iron produces magnetic flux. If the conductive metal plate moves inside the magnetic flux, eddy current is generated inside the metal plate and interacts with the magnetic flux so as to generate damping force.

This paper presents a design procedure of an ECD type RFC mechanism for a linear motor motion stage. A mathematical model of the ECD and an equation of motion for the RFC mechanism with ECD are derived based on lumped parameter analysis. An iterative design procedure for the ECD type RFC mechanism is proposed. A design example shows that the location and width of the ECD as well as the dummy mass can be determined so as to minimize both the size of the linear motor motion stage and the reaction force transmissibility.

2. RFC Mechanism Based on ECD

2.1 Principle

Spring and ECD type RFC mechanisms are shown in Fig. 1. Both RFC mechanisms consist of a movable magnet track with dummy mass and supporting elements (either springs or an ECD). In particular, ECDs (or conductor plates) at both ends of the magnet track effectively produce force to limit the magnet track motion.

An ECD type RFC mechanism has several advantages compared with spring based RFC, as shown in Table 1. Although the ECD has a

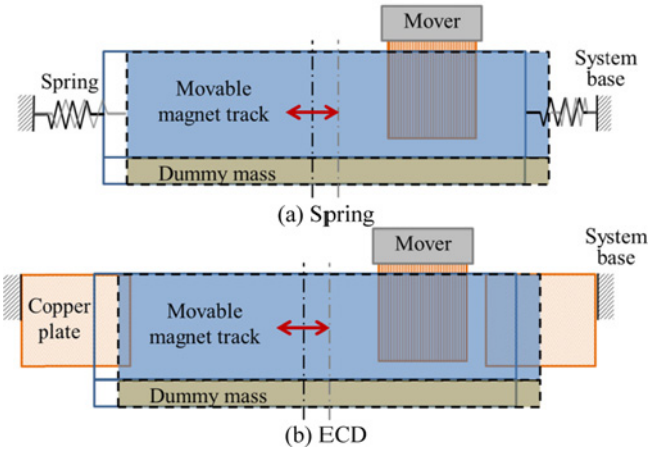

Fig. 1 Passive reaction force compensation mechanisms

Table 1 Comparison of spring and ECD type RFC

Items	Spring-Type	ECD-Type
Main RFC	Spring	ECD
Assistant	ECD(damping)	Spring(homing)
Linearity	Linear	Nonlinear
Resonance	Yes	No
Auto-Homing	Yes	No
Design freedom	Limited	Unlimited
Difficulty of design	Low	High
Manufacturing cost	High	Low

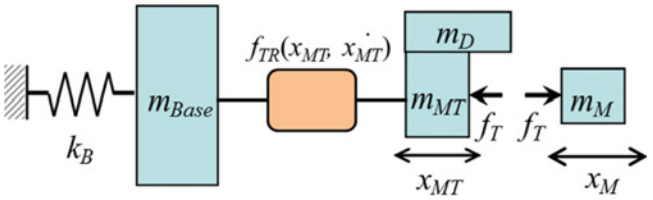

Fig. 2 Dynamic model of the passive RFC mechanism

nonlinear characteristic related to the displacement of the magnet track, the RFC mechanism with an ECD has no resonance, high design freedom, and a low assembly and manufacturing cost. However, design and analysis of the ECD is very difficult and there may be a homing problem with the magnet track due to guide friction.

2.2 Modeling

Both RFC mechanisms can be modeled as in Eq. (1) with transmitted force of either springs or ECD for magnet track as f_{TR}, as shown in Fig. 2. The mover (m_{MT}) moves to a certain position (x_M) according to thrust force (f_T). Then, the magnet track (m_{MT}) with dummy mass (m_D) moves (x_{MT}) freely with respect to the system base (m_{Base}) due to the reaction force (f_T) and transmits reaction force through either the spring or ECD. While the transmitted force of the spring for the magnet track can simply be expressed with $f_{TR} = k_{MT} x_{MT}$ in the case of the springs, the transmitted force of the ECD for the magnet track is complex, details of which will be provided later, Part of the reaction force or transmitted force is transferred to the machine base through the spring or ECD, as shown in Eq. (1).

$$(m_{MT} + m_D)\ddot{x}_{MT} + f_{TR}(x_{MT}, \dot{x}_{MT}) = f_T(t) \quad (1)$$

If the transmitted force consists of damping and stiffness like in Eq. (2), the two main performance indices, magnet track displacement and transmissibility for the RFC mechanism, can be expressed with Eqs. (3) and (4).[5,6] The maximum of the two indices should be less than certain values. While stiffness (k_{MT}) and dummy mass (m_D) are adjusted to meet performance requirements of the spring-type RFC, damping (c_{MT}) and dummy mass (m_D) are variable to satisfy the performance requirements of ECD-type RFC. ECD-type RFC is more effective at suppressing high harmonic terms in motion profiles.[6,7] In addition, an accurate model of an ECD is needed to design an ECD-type RFC since damping of an ECD is not constant but a complex function of magnet track motion and the varying magnetic flux of the magnet track.

$$f_{TR}(x_{MT},\dot{x}_{MT}) = c_{MT}\dot{x}_{MT} + k_{MT}x_{MT} \tag{2}$$

$$\frac{X_{MT}(s)}{F_T(s)} = \frac{1}{((m_{MT}+m_D)s^2 + c_{MT}s + k_{MT})} \tag{3}$$

$$\frac{F_{TR}(s)}{F_T(s)} = \frac{c_{MT}s + k_{MT}}{((m_{MT}+m_D)s^2 + c_{MT}s + k_{MT})} \tag{4}$$

2.3 Mathematical Model of ECD

The ECD force (f_{ECD}) of a moving conductor plate in a constant magnetic field can be expressed as Eq. (5) and is proportional to the geometric coefficient (α), the square of magnetic flux density (B), conductivity (σ), thickness (t), height (l), width (w) and the velocity of the conductor (v).

$$f_{ECD} = \alpha\sigma r B^2 lwv \tag{5}$$

In the case of an ECD type RFC mechanism, the effective width of the ECD changes according to the magnet track motion, and the width and location of the conductor plate. If the conductor plate is completely inside of the magnet track, the effective width is the same as the width of the conductor plate irrespective of the magnet track motion. However, the effective width of the ECD depends on the magnet track motion if the conductor plate is partially inside of the magnet track, as in Fig. 3(a).

The magnet track has sinusoidal magnetic flux density along the motor moving direction. Alternating the arrangement of the south and north poles of a permanent magnet produces sinusoidal magnetic flux density as shown in Fig. 3(b). The magnetic flux density varies according to the inner position of the magnet track (there is more harmonics farther from the center position), just pure sinusoidal magnetic flux density is assumed. This sinusoidal magnetic flux interacts with the three phase currents of the mover coil to generate the thrust force.

ECD force can be calculated by considering its effective width and sinusoidal magnetic flux density using Eq. (6). Final expressions may be different according to the magnet track motion since the effective width varies according to the magnet track position which changes integration range s correspondingly.

$$f_{ECD} = \alpha\sigma r l B^2 \dot{x}_{MT} \int \sin^2\left(\frac{\pi}{p}x\right) dx \tag{6}$$

The ECD force with various magnet track motions is shown in Fig. 4. The magnet track positions with respect to the ECD are illustrated graphically in the upper part of Fig. 3(a) (The blue rectangle denotes the magnet track while the orange rectangle denotes the ECD). The forces of two copper plates are summed and its damping coefficient varies according to the magnet track motion.

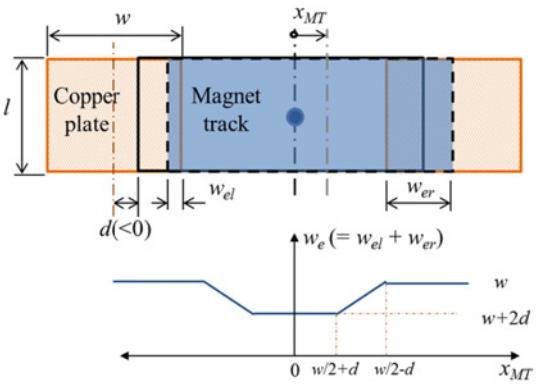

(a) Effective width of the ECD

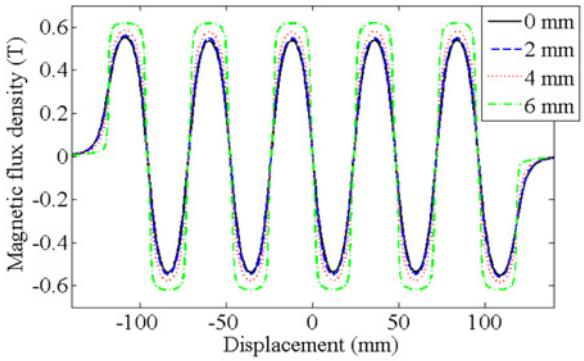

(b) Magnetic flux density at various inner positions of magnet track

Fig. 3 Magnetic flux density of the magnet track

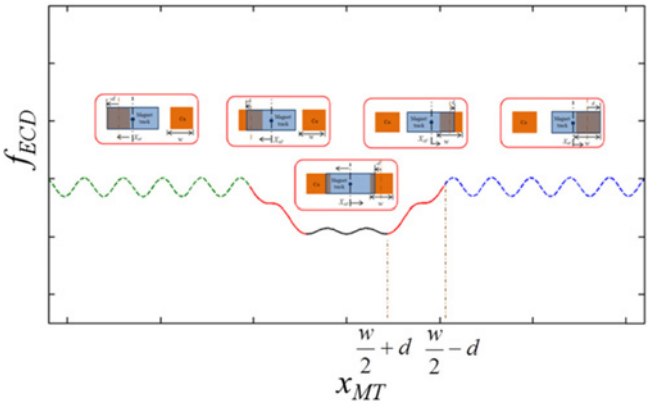

Fig. 4 ECD force according to the magnet track motion

2.4 Experimental Verification

The experimental set-up is built to verify the mathematical model of the ECD, as shown in Fig. 5. The experimental set-up is based on a linear motor stage (517 mm stroke, max acc. 20 m/s^2, max speed 5.0 m/s continuous 240 N, Resolution 1.0 μm) and the small magnet track is mounted on the mover. One end of a load cell (max. 50 kgf) is assembled with a copperplate (or ECD) while the other end of the load

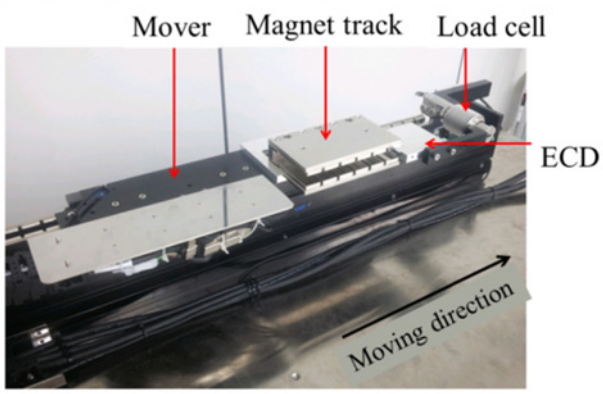

Fig. 5 Experimental set-ups to verify the model of the ECD

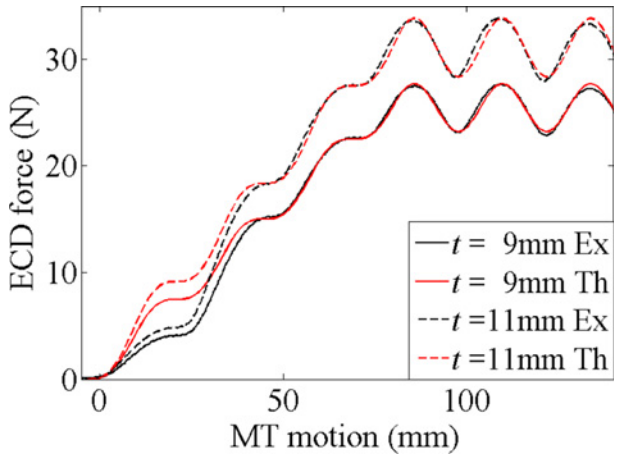

Fig. 6 Experimental validation of ECD model

cell is fixed to the housing. ECD force is measured by the load cell while there is a constant speed motion of the magnet track.

Experimental measurements and mathematical calculations of the ECD force of a single copper plate are compared in Fig. 6. The mover moves with constant speed (100 mm/s) and the ECD forces of copper plates with both 9 and 11 mm thickness are measured. Since the magnetic flux is not uniform inside of the magnet track, as shown in Fig. 3(b), and the width of the copper plate affects both the static and sinusoidal magnitude of the ECD, as shown in Table A1, the ECD width is increased about 10% in order to match both the static and sinusoidal magnitudes of the ECD force.

3. Design of ECD Type RFC Mechanism

3.1 Procedure

The principle of optimal design of an ECD type RFC mechanism is shown in Fig. 7. There are two design objectives: minimizing both the dummy mass and the stage size. First, specifications of a linear motion stage such as maximum thrust force are required. Based on the specifications of the linear motion stage, couples of motion profiles are chosen for specific applications and determine performance indices of the RFC mechanism: force transmissibility and maximum displacement of the magnet track. Then, initial dummy mass is assumed for the magnet track and location and width of the ECD are determined to

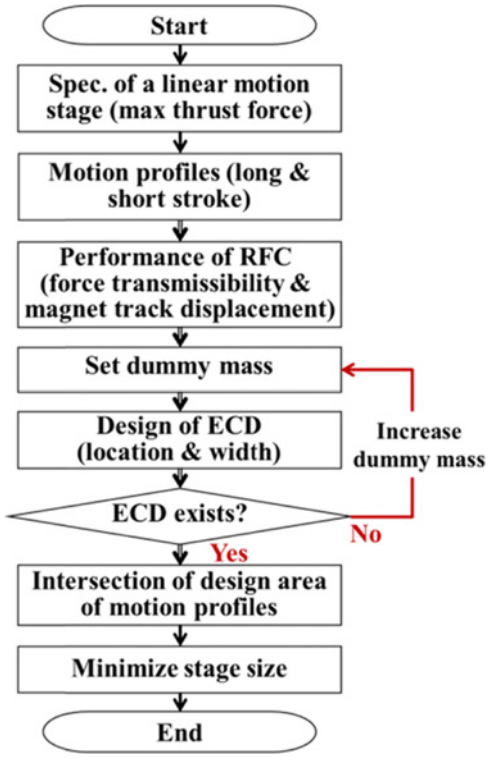

Fig. 7 Design procedure of the ECD type passive RFC mechanism

satisfy two performance indices. If there is no proper ECD design, the dummy mass increases and both performance indices meet design requirements. If there is a set of suitable ECD designs, the intersection of the ECD design for the motion profiles can be found and both a location and the width of ECD can finally be determined so as to minimize the motion stage size.

3.2 Stage System Parameters

Thrust force can be divided into force for motion profile and force against mover friction, as shown in Eq. (7). Here, f_m is the thrust force for the mover motion or motion profile itself (product of mass of the mover and acceleration of the motion profile) and f_f is required force due to friction and the cables of the mover (Eq. (8)). The guide friction of the magnet track is approximated as viscous damper (c_{MT}) since the magnet track is supported by a linear guide with low friction.

$$f_T = f_m + f_f \tag{7}$$

$$f_f(\dot{x}_M) = f_{fc}\mathrm{sgn}(\dot{x}_M) + f_{fs}e^{-n_s\left|\frac{\dot{x}_M}{v_s}\right|}\mathrm{sgn}(\dot{x}_M) + k_v\dot{x}_M \tag{8}$$

Here, f_{fc} is Coulomb friction force, f_{fs} is the difference between max static and Coulomb friction forces, n_s is the exponent coefficient for Stribeck effect, and v_s is Stribeck velocity.

All parameters of the passive RFC mechanism are identified experimentally and are shown in Table 2. An ECD type RFC mechanism is installed for a linear motor motion stage with max 400 N and about 500 mm stroke, which is shown in Fig. 8(a). If the cover of the stage is removed, the magnet track, ECD and spring can be seen from behind, as shown in Fig. 8(a). The free vibration of the magnet

Table 2 Parameters of the passive RFC mechanism

Parameter	Value	Parameter	Value
m_{MT}	21 kg	f_{fc}	1 N
k_{MT}	1200 N/m	f_{fs}	6 N
c_{MT}	37 Ns/m	n_s	0.01
k_v	30 Ns/m	v_s	0.1 m/s

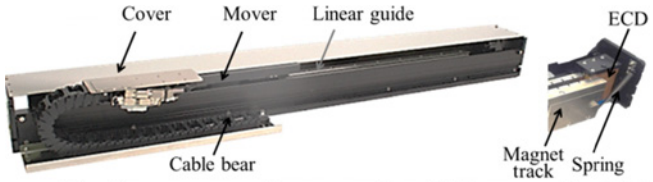

(a) Linear motor motion stage with an ECD type passive RFC

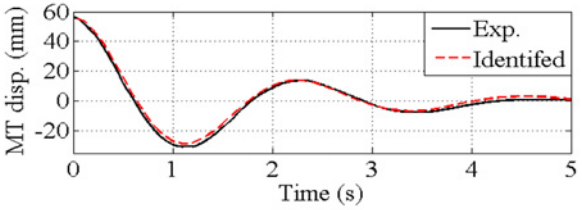

(b) Identification of model parameter of the magnet track

Fig. 8 ECD type passive RFC mechanism and its identification

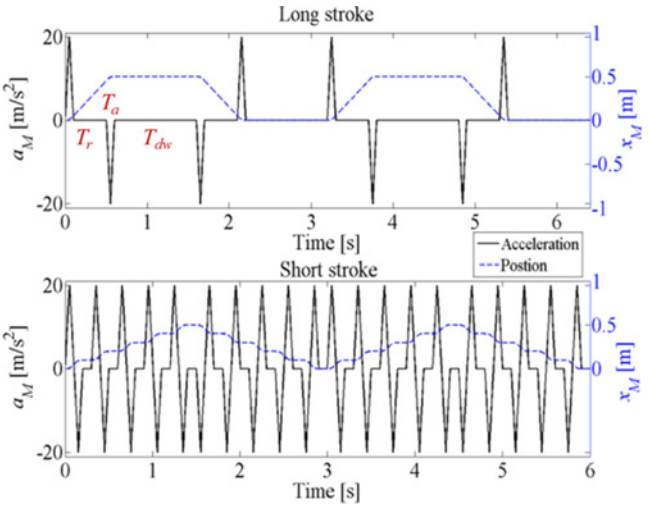

Fig. 9 Two typical motion profiles for linear motion stage

track is experimentally measured using a built-in hall sensor array.[17] Although a detailed procedure of the identification, including a friction model, is out of the scope of this paper, its identification results for the magnet track motion measurement are shown in Fig. 8(b).

Typical repetative motion profiles used in a linear motor motion stage are considered: ping-pong (back and forth) motion, repetitive go-and-stop motion and combined motions. Fig. 9 shows both a long stroke ping-pong motion (accleration time T_a is 0.05 s, run time T_r is 0.4 s ,dwell time T_{dw} is 1 s and peak acceleration is 20 m/s^2) and a repetitive go-and-stop motion (accleration time T_a is 0.1 s, run time T_r is 0 s ,dwell time T_{dw} is 0.1 s and peak acceleration is 20 m/s^2).

3.3 Design Example

The performance indexes of the RFC are as follows: force transmissibility is 50% and maximum displacement of the magnet track

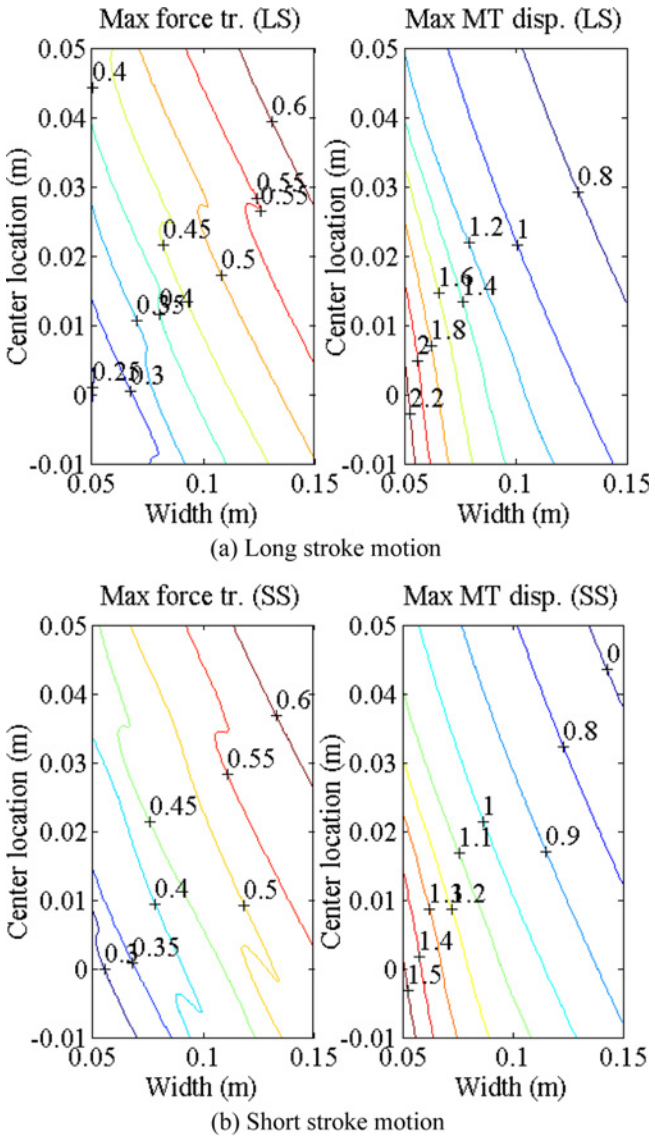

Fig. 10 Performance indexes of the ECD type RFC mechanism for long and short motion profiles

is 0.06 m. A simulation model is built to design an ECD type passive RFC mechanism. The simulation model contains thrust force, a mathematical model of the RFC mechanism and a calculation of force transmissibility. Thrust force is calculated considering the mover motion and identified friction force. Then, the magnet track motion is calculated with Eq. (1) considering a mathematical model of the ECD (Appendix A). In particular, an experimentally-verified mathematical model of the ECD is used.

For two motion profiles, there are two performance indices: force transmissibility (f_{TR}/f_T) and maximum normalized magnet track displacement ($x_{MT}/0.06$) are calculated according to various locations and widths of the ECD as shown in Fig. 10. From two performance indices, the design area of the ECD type RFC mechanism is determined for two motion profiles and shown in Fig. 11. If the dummy mass increases, the limit of the force transmissibility moves up and that of the magnet track displacement moves down creating an intersection of two requirements. Finally, the dummy mass is determined as 21 kg. The long stroke motion has a smaller

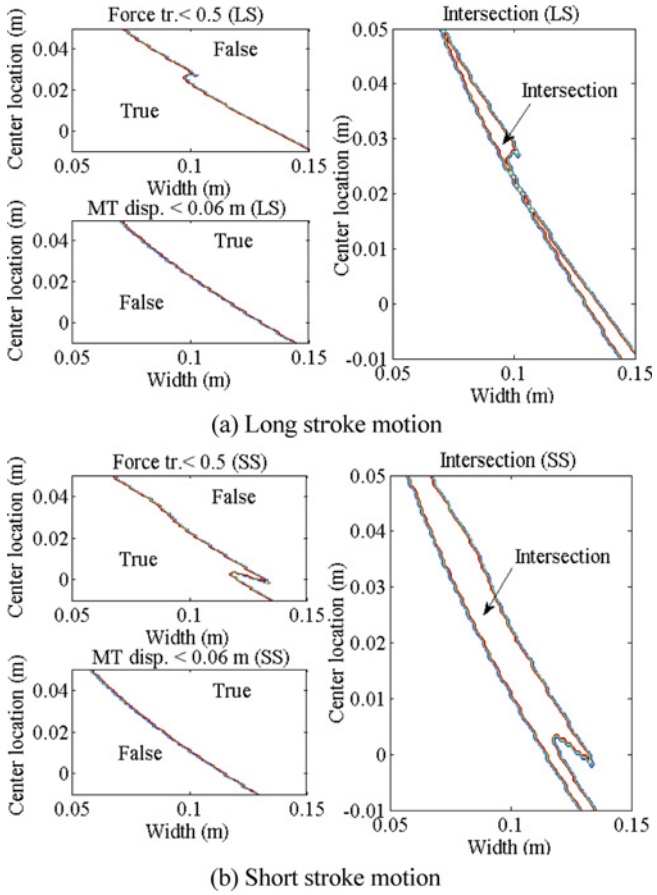

Fig. 11 Design area of an ECD type RFC mechanism for two motion profiles

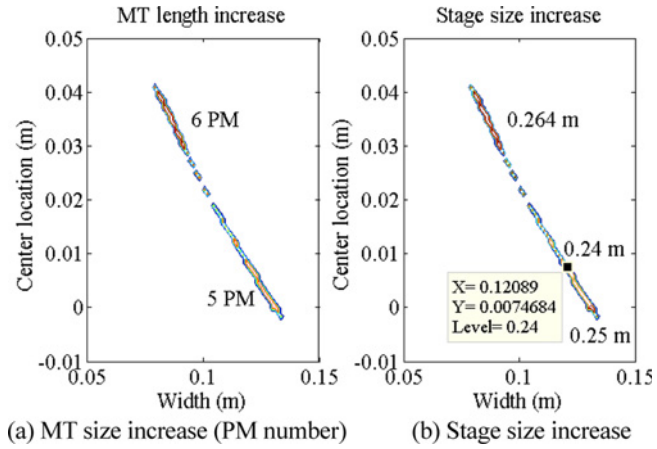

Fig. 12 Location and width of ECD to minimize the size of the linear motion stage

intersection area than the short stroke motion due to the greater energy of the long stroke motion.[9]

The location and width of the ECD can be determined from a set of possible ECD designs to minimize the size of the linear motion stage, as shown in Fig. 12. First, a common design area can be determined from the design area of two motion profiles. Then, the overlapping length of the magnet track and the ECD is calculated to determine how many additional permanent magnets are required, as shown in Fig. 12(a). The ECD type RFC mechanism needs 5 or 6 additional permanent magnets. A wider ECD with its center farther from the magnet track needs a smaller number of permanent magnets. Finally, the size increase of the linear motion stage due to the ECD type RFC mechanism can be calculated. The size increase of the stage depends on the number of additional permanent magnets, the width and location of the ECD, as well as the maximum magnet track displacement. The stage size increases again if the center location of the ECD moves too far from the magnet track, as shown in Fig. 12(b). Finally, the width and location of the ECD are decided as 120 mm and 7.5 mm, respectively and the stage with the ECD type RFC mechanism has a 240 mm size increase compared to a linear motor motion stage without a RFC.

4. Conclusions

This paper presents a design procedure of an ECD type RFC mechanism for a linear motor motion stage. The ECD type RFC mechanism overcomes the disadvantages of the spring type RFC mechanism such as resonance and assembly difficulties due to the spring. First, a lumped parameter model of the ECD for RFC mechanism is derived and verified by measuring the ECD force experimentally. Then, an iterative design procedure for an ECD type RFC mechanism is proposed based on the lumped parameter model. Finally, a design example shows that the location and width of the ECD, as well as dummy mass, can be determined to minimize both the size of the linear motor motion stage and the reaction force transmissibility.

ACKNOWLEDGEMENT

This work was by Basic Science Research Program through the National Research Foundation of Korea (NRF) funded by the Ministry of Education, Science and Technology (NRF-2013R1A1A2010764).

REFERENCES

1. ASML, “TWINSCAN NXT:1960Bi,” http://www.asml.com/asml/show.do?lang=EN&ctx=46772&dfp_product_id=7414 (Accessed 21 December 2015)
2. Singhose, W., “Command Shaping for Flexible Systems: A Review of the First 50 Years,” Int. J. Precis. Eng. Manuf., Vol. 10, No. 4, pp. 153-168, 2009.
3. Iwasaki, M., Seki, K., and Maeda, Y., “High-Precision Motion Control Techniques: A Promising Approach to Improving Motion Performance,” Industrial Electronics Magazine, Vol. 6, No. 1, pp. 32-40, 2012.
4. Arakelian, V. H. and Smith, M., “Shaking Force and Shaking Moment Balancing of Mechanisms: A Historical Review with New Examples,” Journal of Mechanical Design, Vol. 127, No. 2, pp. 334-339, 2005.

5. Greene, P. M., Hero, S., and Bittner, D., "Reaction Force Transfer System," US Patent, No. US006844635B2, 2005.

6. Galburt, D. N., "Method, System, and Apparatus for Management of Reaction Loads in a Lithography System," US Patent, No. US006784978B2, 2004.

7. Ka, A., Poon. T., Wai, L., Kho, F., Yang, P.-H., et al., "Modular Stage with Reaction Force Cancellation," US Patent, No. US006917412B2, 2005.

8. Cho, K.-J., Choi, D.-S., and Ahn, H.-J., "Mechanism and Control of Reaction Force Compensation of XY Linear Motion Stage System," Transactions of the Korean Society of Mechanical Engineers: A, Vol. 35, No. 6, pp. 599-607, 2011.

9. You, Y.-H. and Ahn, H.-J., "A Passive Reaction Force Compensation (RFC) Mechanism for a Linear Motor Motion Stage," Int. J. Precis. Eng. Manuf., Vol. 15, No. 5, pp. 797-801, 2014.

10. Nguyen, D. C. and Ahn, H.-J., "Dynamic Analysis and Iterative Design of a Passive Reaction Force Compensation Device for a Linear Motor Motion Stage," Int. J. Precis. Eng. Manuf., Vol. 15, No. 11, pp. 2367-2373, 2014.

11. Nguyen, D. C. and Ahn, H.-J., "A Fuzzy-P Controller of an Active Reaction Force Compensation (RFC) Mechanism for a Linear Motor Motion Stage," Int. J. Precis. Eng. Manuf., Vol. 16, No. 6, pp. 1067-1074, 2015.

12. Ahn, H.-J., You, Y., Kim, K., Kwon, J., Cho, K., et al., "Multi-Physical Analysis of Eddy Current Damper (ECD) for Reaction Force Compensation Device," Applied Mechanics and Materials, Vol. 300-301, pp. 920-923, 2013.

13. Sodano, H. A., Bae, J.-S., Inman, D. J., and Belvin, W. K., "Concept and Model of Eddy Current Damper for Vibration Suppression of a Beam," Journal of Sound and Vibration, Vol. 288, No. 4, pp. 1177-1196, 2005.

14. Sodano, H. A., Bae, J.-S., Inman, D. J., and Belvin, W. K., "Improved Concept and Model of Eddy Current Damper," Journal of Vibration and Acoustics, Vol. 128, No. 3, pp. 294-302, 2006.

15. Ebrahimi, B., Khamesee, M. B., and Golnaraghi, F., "Eddy Current Damper Feasibility in Automobile Suspension: Modeling, Simulation and Testing," Smart Materials and Structures, Vol. 18, No. 1, Paper No. 015017, 2009.

16. Chen, W., Jiang, J., Liu, J., Bai, S., and Chen, W., "A Passive Eddy Current Damper for Vibration Suppression of a Force Sensor," Journal of Physics D: Applied Physics, Vol. 46, No. 7, Paper No. 075001, 2013.

17. Ahn, H.-J. and Kim, K. R., "2D Hall Sensor Array for Measuring the Position of a Magnet Matrix," Int. J. Precis. Eng. Manuf.-Green Tech., Vol. 1, No. 2, pp. 125-129, 2014.

APPENDIX A

ECD force has different characteristic according to its width and center location. The lumped ECD force is calculated for width and center locations of the ECD: (a) complete outside (d<0, $|d|$>w/2), (b) partial outside (d>0, $|d|$<w/2), (c) complete inside (d>0, $|d|$>w/2), as shown in Fig. A1. The partial inside case (d<0, $|d|$<w/2) is already shown in Fig. 3. The lumped ECD force of Eq. (6) is calculated according to four cases of ECD location and width and shown in Table A1.

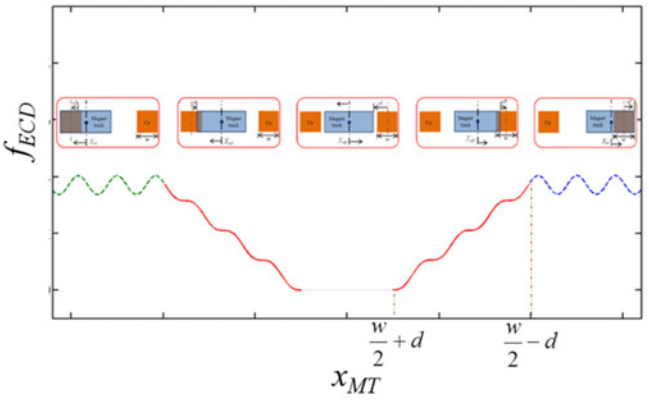

(a) d<0, $|d|$ > w/2

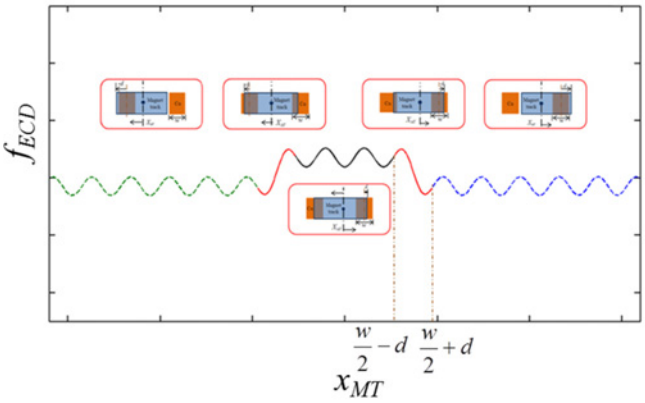

(b) d>0, $|d|$ < w/2

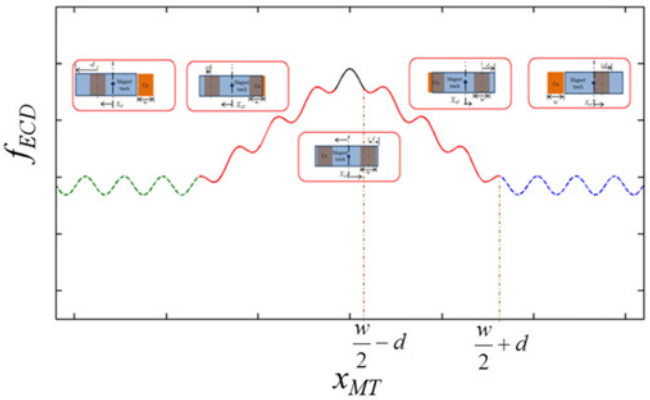

(c) d<0, $|d|$ > w/2

Fig. A1 Approximate ECD force according to displacement of the magnet track

Table A1 ECD force according to location and width of ECD

ECD location	Magnet track motion range	ECD force
Complete outside of MT $d<0$ $\lvert d\rvert>\frac{w}{2}$	$-\left(-d-\frac{w}{2}\right)\le x_{MT}\le -d-\frac{w}{2}$	0
	$\left(-d-\frac{w}{2}\right)\le x_{MT}\le \frac{w}{2}-d$	$\alpha\sigma t l B^2 \dot{x}_{MT}\left[\frac{1}{2}\left(\frac{w}{2}+d+x_{MT}\right)-\frac{p}{4\pi}\sin\left(\frac{2\pi}{p}\left(\frac{w}{2}+d+x_{MT}\right)\right)\right]$
	$\frac{w}{2}-d\le x_{MT}$	$\alpha\sigma t l B^2 \dot{x}_{MT}\left[\frac{w}{2}-\frac{p}{2\pi}\sin\left(\frac{w\pi}{p}\right)\cos\left(\frac{2\pi}{p}(x_{MT}+d)\right)\right]$
Partial inside of MT $d<0$ $\lvert d\rvert<\frac{w}{2}$	$-\left(-d-\frac{w}{2}\right)\le x_{MT}\le \left(-d-\frac{w}{2}\right)$	$\alpha\sigma t l B^2 \dot{x}_{MT}\left[\left(\frac{w}{2}+d\right)-\frac{P}{2\pi}\sin\left(\frac{w\pi}{p}\right)\cos\left(\frac{2\pi}{p}(x_{MT}+d)\right)\right]$
	$\left(-d-\frac{w}{2}\right)\le x_{MT}\le \frac{w}{2}-d$	$\alpha\sigma t l B^2 \dot{x}_{MT}\left[\frac{1}{2}\left(\frac{w}{2}+d+x_{MT}\right)-\frac{p}{4\pi}\sin\left(\frac{2\pi}{p}\left(\frac{w}{2}+d+x_{MT}\right)\right)\right]$
	$\frac{w}{2}-d\le x_{MT}$	$\alpha\sigma t l B^2 \dot{x}_{MT}\left[\frac{w}{2}-\frac{p}{2\pi}\sin\left(\frac{w\pi}{p}\right)\cos\left(\frac{2\pi}{p}(x_{MT}+d)\right)\right]$
Partial outside of MT $d>0$ $\lvert d\rvert<\frac{w}{2}$	$-\left(\frac{w}{2}-d\right)\le x_{MT}\le \left(\frac{w}{2}-d\right)$	$\alpha\sigma t l B^2 \dot{x}_{MT}\left[\left(\frac{w}{2}+d\right)-\frac{p}{2\pi}\sin\left(\frac{2\pi}{p}\left(\frac{w}{2}+d\right)\right)\cos\left(\frac{2\pi}{p}x_{MT}\right)\right]$
	$\left(\frac{w}{2}-d\right)\le x_{MT}\le \frac{w}{2}+d$	$\alpha\sigma t l B^2 \dot{x}_{MT}\left[\frac{1}{2}\left(\frac{3w}{2}+d-x_{MT}\right)-\frac{p}{2\pi}\sin\left(\frac{w\pi}{p}\right)\cos\left(\frac{2\pi}{p}(d+x_{MT})\right)-\frac{p}{4\pi}\sin\left(\frac{2\pi}{p}\left(\frac{w}{2}+d-x_{MT}\right)\right)\right]$
	$\frac{w}{2}+d\le x_{MT}$	$\alpha\sigma t l B^2 \dot{x}_{MT}\left[\frac{w}{2}-\frac{p}{2\pi}\sin\left(\frac{w\pi}{p}\right)\cos\left(\frac{2\pi}{p}(x_{MT}+d)\right)\right]$
Complete inside of MT $d>0$ $\lvert d\rvert>\frac{w}{2}$	$-\left(d-\frac{w}{2}\right)\le x_{MT}\le \left(d-\frac{w}{2}\right)$	$\alpha\sigma t l B^2 \dot{x}_{MT}\left[w-\frac{p}{\pi}\sin\left(\frac{w\pi}{p}\right)\cos\left(\frac{2\pi}{p}d\right)\cos\left(\frac{2\pi}{p}x_{MT}\right)\right]$
	$\left(d-\frac{w}{2}\right)\le x_{MT}\le d+\frac{w}{2}$	$\alpha\sigma t l B^2 \dot{x}_{MT}\left[\frac{1}{2}\left(\frac{3w}{2}+d+x_{MT}\right)-\frac{p}{2\pi}\sin\left(\frac{w\pi}{p}\right)\cos\left(\frac{2\pi}{p}(d+x_{MT})\right)-\frac{p}{4\pi}\sin\left(\frac{2\pi}{p}\left(\frac{w}{2}+d-x_{MT}\right)\right)\right]$
	$d+\frac{w}{2}\le x_{MT}$	$\alpha\sigma t l B^2 \dot{x}_{MT}\left[\frac{w}{2}-\frac{p}{2\pi}\sin\left(\frac{w\pi}{p}\right)\cos\left(\frac{2\pi}{p}(x_{MT}+d)\right)\right]$